Ionized impurity scattering in periodically δ-doped InP

A. B. Henriques, L. C. D. Gonçalves, and N. F. Oliveira, Jr.
Instituto de Física, Universidade de São Paulo, Caixa Postal 66318, 05315-970 São Paulo, Brazil

P. L. Souza and B. Yavich
Centro de Estudos em Telecomunicações, Pontifícia Universidade Católica, Rua Marques de São Vicente 225, 22453-900 Rio de Janeiro, Brazil

(Received 5 November 1996)

The quantum mobility in the individual minibands of InP with periodic Si δ doping was estimated from the Shubnikov–de Haas spectra of the samples, measured at 4.2 K in fields of 0–14 T. The set of samples studied had a sheet density of Si atoms of about 4.9×10^{12} cm^{-2} in each doped layer, and a doping period in the range 90–300 Å. A theoretical model for the quantum mobility in individual minibands was developed, and theoretical estimates of the quantum mobility are in reasonable agreement with the experimental values. It is observed that at a fixed doping period the quantum mobilities increase with the index of the miniband, and the quantum mobility in an individual miniband decreases when the doping period is made shorter. The dependence of the quantum mobility on the miniband index and doping periodicity correlates with the dependence of the mean distance between electrons and the doped layer on the same quantities. These results demonstrate that in δ-doped semiconductors the binding length of the quantum-confined electronic charge is a very important parameter, determining the carrier mobility which can be attained in these systems. [S0163-1829(97)01119-3]

I. INTRODUCTION

Semiconductors in which the atoms of the dopants are concentrated around a single plane of the host crystal lattice have important technological applications and display interesting physical properties.[1,2] Using epitaxial growth techniques such as metal-organic vapor phase epitaxy (MOVPE) and molecular-beam epitaxy, planar doping (or δ doping) with silicon has been accomplished for various III-V semiconductors, for instance, GaAs, $Al_xGa_{1-x}As$, InSb, and InP. In semiconductors doped periodically with sheets of Si, the carriers released from the shallow donor Si atoms are confined by a periodical space charge potential, which splits the continuous conduction band of the host semiconductor into a set of electronic minibands. The conductivity parallel to the doped layer is dominated by carriers confined in such minibands: these carriers interact strongly with the charged donor atoms located in the doped regions, and this interaction consists the mechanism which limits the carrier mobility in δ-doped systems.[3–5]

From the theoretical standpoint, calculations of the electronic mobility in samples with a single δ layer have been made using either the Thomas-Fermi model[6–8] or the random-phase approximation (RPA) (Refs. 8–12) to describe the screened interaction between confined carriers and ionized impurities. The theoretical calculations made in the frame of the RPA show good quantitative agreement with experimental estimates,[9,11] while the agreement is poorer when a two-dimensional Thomas-Fermi model of screening is used (see Ref. 13 by some of the authors). However, to the best of our knowledge a calculation of the electronic mobilities in periodically δ-doped samples has not yet been attempted, and this is the purpose of the present study. For the periodically δ-doped semiconductor, the theoretical quantum mobility calculation is based on the same input quantities as the mobility theory for semiconductors with a single δ-doped layer, i.e., electronic energy spectrum and wave functions, and a model for the screened electrostatic potential of ionized impurities. The basic novelty is in the form electronic wave functions, which for a periodically δ-doped system are described by Bloch states, whereas for a semiconductors with a single δ layer the wave functions describe states which are spatially localized around the doped layer. Our calculations were made using the RPA model for the screened Coulomb interaction between carriers and ionized donors; this choice was motivated by the success of the RPA theory in describing the carrier mobility in δ-doped materials with a single δ-doped layer.

II. THEORY OF MINIBAND QUANTUM MOBILITIES IN THE RPA APPROXIMATION

In this section effective atomic units are used, whereby the units of mass, length, and energy are the effective mass m^*, the effective Bohr radius $a_B=\epsilon\hbar^2/m^*\kappa e^2$, and the effective Hartree $H=\hbar^2/m^*a_B^2$, respectively. For InP, we assume $m^*=0.08\ m_0$ (Ref. 14) and $\epsilon=11.8$,[15] which gives $a_B=78$ Å and $H=15.7$ meV.

When electrons are confined by a potential which is periodic along one axis (the growth direction z), as occurs in a semiconductor with a periodical δ doping, the electronic states are quantized into superlattice minibands of energies $E(n,k_\perp,k)$,

$$E(n,k_\perp,k)=E_n(k)+\tfrac{1}{2}k_\perp^2,$$

where $\vec{k}_\perp$ and k are the wave-vector components perpendicular and parallel to the growth axis, respectively, and $E_n(k,z)$ is the miniband dispersion. In order of increasing energy, we will denote the succession of minibands as $E1$,

$E2, E3, \ldots$. The electronic states corresponding to the energies $E_n(k,z)$ are described by the wave functions

$$\Psi_n(\vec{k}_\perp,k,\vec{\rho},z)=\frac{e^{i\vec{k}_\perp\cdot\vec{\rho}}}{\sqrt{S}}\chi_n(k,z), \tag{1}$$

where S is the area of the sample, $\chi_n(k,z)=u_n(k,z)e^{ikz}$, and $u_n(k,z)$ are Bloch functions normalized to the length of the superlattice. Functions $\chi_n(k,z)$ are the solutions of the Schrödinger equation

$$-\frac{1}{2}\frac{d^2}{dz^2}\chi_n(z)+[V_H(z)+V_{\rm xc}(z)]\chi_n(k,z)=E_n(k)\chi_n(k,z) \tag{2}$$

where $V_{\rm xc}(z)$ is local density approximation for the exchange-correlation correction to the confining potential, which was taken to be equal to the form due to Hedin and Lundqvist,[16]

$$V_{\rm xc}(z)=\frac{1}{\pi\alpha r_s}[1+0.7734x\ln(1+x^{-1})].$$

$\alpha=(4/9\pi)^{1/3}$, $r_s=[4/3\pi n(z)]^{-1/3}$, $x=r_s/21$, and $V_H(z)$ is the self-consistent Hartree potential, which is obtained from a numerical solution of the Poisson equation

$$\frac{d^2V_H(z)}{dz^2}=4\pi[n_d(z)-n(z)], \tag{3}$$

where $n_d(z)$ is the density of ionized donors, $n(z)=(1/\pi)\Sigma_{nk}|u_n(k,z)|^2\phi_{nk}\Theta(\phi_{nk})$ is the density of free carriers, $\phi_{nk}=\phi-E_n(k)$, ϕ denotes the Fermi energy, and

$$\Theta(x)=\begin{cases}1 & \text{if } x>0\\ 0 & \text{otherwise}\end{cases}$$

is the Heaviside step function.

The scattering rate of electrons from a given quantum state for $T=0$ K can be obtained from the Fermi golden rule, taking the Coulomb interaction between electrons and ionized impurities to be the scattering mechanism. By using the wave functions given by Eq. (1), and considering the scattering processes of carriers at the Fermi surface, for the quantum lifetime of the state k of the nth electronic miniband (in atomic units, the quantum lifetime equals the quantum mobility μ_Q), one obtains

$$\mu_Q^{-1}(n,k)=\frac{S}{\pi}\sum_{n',k'}\int_0^{\pi}\overline{|V^{\rm TOT}_{nk,n'k'}(q_{nk,n'k'})|^2}d\varphi, \tag{4}$$

where the summation extends over the quantum states (n',k') which lie below the Fermi level (i.e., $\phi_{n'k'}>0$),

$$q_{nk,n'k'}=2^{1/2}[\phi_{nk}+\phi_{n'k'}-2\sqrt{\phi_{nk}\phi_{n'k'}}\cos\varphi]^{1/2},$$

the integration variable φ is the angle of scattering formed between vectors $\vec{k}_\perp$ and $\vec{k}'_\perp$, and

$$\overline{|V^{\rm TOT}_{nk,n'k'}(q)|^2}=\left(\frac{2\pi}{q}\right)^2\frac{N_d}{S}\sum_{t=-\infty}^{+\infty}\left|\sum_{mlm'l'}\epsilon^{-1}_{nkn'k',mlm'l'}(q)\times\int_0^{N\,d}\chi_m(l,z)\chi^*_{m'}(l',z)e^{-q|z-td|}dz\right|^2$$

represents the statistical average of the matrix elements of the two-dimensional Fourier transform of the scattering potential. In the latter equation the summation extends over all the electronic energy levels, N_d is the areal density of single charged donor atoms in each doping period, distributed along the z direction in a plane of zero thickness; d is the superlattice period; $N\,d$ is the Born–von Karman period; and $\epsilon_{nkn'k',mlm'l'}(q)$ is the dielectric matrix which is given by

$$\epsilon_{nkn'k',mlm'l'}(q)=\delta_{nm}\delta_{kl}\delta_{n'm'}\delta_{k'l'}+A_{mlm'l'}(q)\;T_{nkn'k',mlm'l'}(q),$$

with $A_{mlm'l'}(q)$ being the independent response particle density matrix, given in the Appendix of Ref. 17, and $T_{nkn'k',mlm'l'}(q)$ is the Coulomb energy form factor

$$T_{nkn'k',mlm'l'}(q)=\frac{2\pi}{q}\int_0^{N\,d}\chi_n(k,z)\chi^*_{n'}(k',z)\times\chi^*_m(l,z')\chi_{m'}(l',z')e^{-q|z-z'|}dz\;dz'.$$

In order to test the theory, a comparison with the quantum mobility obtained experimentally is needed. The quantum mobility of carriers in individual minibands can be extracted from the Shubnikov–de Haas (SdH) spectrum. As shown in Refs. 18 and 19, in a semiconductor superlattice each miniband manifests itself in the SdH experiment as a separate set of oscillatory components. Every miniband can be assigned to one of three categories: those of two-dimensional character and vanishing bandwidth, $\Delta_n=0$; those of quasi-two dimensional character, described by a small dispersion and narrow bandwidth, $\Delta_n<\phi_n$, and those effectively three-dimensional, $\Delta_n>\phi_n$, where ϕ_n represents the energy distance between the Fermi level and the threshold of the miniband.

The contribution to the magnetoresistance of a miniband whose bandwidth is smaller than its Fermi energy, i.e. $\Delta_n<\phi_n$, will be described by[19]

$$\frac{\Delta\rho_{xx}}{\rho_0}\sim-\frac{X}{\sinh X}e^{-\alpha_n u}\{2J_0(\beta_n u)\cos\omega_n u+8\,\epsilon_n\Im{\rm m}[e^{-i\beta_n u}\Phi(1/2,2,2i\beta_n u)]\sin\omega_n u\}, \tag{5}$$

where $X=2\pi^2T/B$, T is the temperature in units of $\hbar^2/k_Bm^*a_B^2$, $u=1/B$, $\alpha_n=\pi/\mu_Q(n)$, $\mu_Q(n)$ is the quantum mobility in the nth miniband, $\beta_n=\pi\Delta_n$, $\omega_n=2\pi(\phi_n-\Delta_n)$ and ϵ_n is a dimensionless parameter which is obtained by fitting the numerically calculated dispersion law, $E_n(k)$, to the expression

$$E_n(k)=\frac{\Delta_n}{2}(1-\cos kd)-\epsilon_n\frac{\Delta_n}{2}(1-\cos 2kd). \tag{6}$$

Equation (5) was obtained assuming the quantum mobility to be constant within a miniband. Note also that when the spacing between the doped layers is made very large ($d \to \infty$), the width of the minibands decreases ($\Delta_n \to 0$), and Eq. (5) takes the familiar form associated with an electron gas confined in two dimensions:[20]

$$\frac{\Delta\rho_{xx}}{\rho_0} \sim -2\frac{X}{\sinh X} e^{-\alpha_n u} \cos 2\pi\phi_n u \ . \tag{7}$$

In the most general case, Eq. (5) will be characterized by two oscillatory components, respective to the ''belly'' and ''neck'' extremal orbits of the mini-Fermi surface associated with the miniband; however, as shown in Ref. 19, in periodically δ-doped systems the neck orbit is not detectable. This conclusion is based upon the observation that in order for the neck orbit to be detectable, the energy-level broadening must be smaller than the miniband width *and also* smaller than the minigap to the higher-energy miniband. However, in periodically δ-doped systems these two conditions are never met simultaneously, hence each miniband will manifest itself with a single oscillatory component due to the belly orbit. This assertion leads us to conclude that in the case of periodically δ-doped semiconductors the quantum mobility appearing in Eq. (5) pertains to the belly orbit state. Therefore if we wish to test the quantum mobility theory developed above, the quantum mobility obtained from a fit of Eq. (5) to the experimental data should be compared to the output of Eq. (4) at the wave vector associated with the belly orbit (i.e., $k=0$ for minibands $E1, E3, \ldots$, and $k=\pi/d$ for minibands $E2, E4, \ldots$).

For those minibands whose bandwidth is larger than the Fermi energy, i.e. when $\Delta_n > \phi_n$, the magnetoresistance oscillations can be approximated by the usual expression associated with an unrestrained free electron gas in three dimensions,[21]

$$\frac{\Delta\rho_{xx}}{\rho_0} \sim -2\frac{X}{\sinh X}\ \frac{e^{-\alpha u}}{\sqrt{u}} \cos\left(2\pi\phi_n u - \frac{\pi}{4}\right) \ . \tag{8}$$

The quantum mobility in this case can similarly be obtained by fitting Eq. (8) to the isolated magnetoresistance oscillatory component.

III. EXPERIMENT

The δ-doped structures were grown at 640 °C by low pressure-MOVPE in an AIX 200 reactor at 20 mbar with a growth rate of 4.5 Å/s. The source materials were PH_3 (100%), TMIn (trimethyl indium), and 1% SiH_4 diluted in H_2. On (100) Fe-doped InP substrates, first a 0.3-μm-thick undoped buffer was grown, followed by a periodically δ-doped InP layer, and finally a 500-Å cap layer was deposited. The periodical structures are composed of either five or ten periods, with a spacing varying from 90 to 300 Å. The dopant layers were deposited during a 25-s growth interruption. The silane flux was triggered 2 s after growth interruption, and halted 2 s before the growth was resumed. In order to determine the width of the doped layer and the doping period, the capacitance-voltage profile (C-V) was measured for each sample, using an electrochemical profiler PN4300.

The Shubnikov–de Haas experiment was carried out in a superconducting magnet. The sample was placed in liquid He at 4.2 K. The magnetoresistance measurements were made in the constant-current mode, employing currents of $\sim 10\ \mu$A, and using a four-contact geometry; the samples were approximately square, with contacts in the corners. The magnetoresistance oscillations were measured in magnetic fields of intensity up to 14 T.

IV. RESULTS

We obtained an experimental estimate of the quantum mobility in each of the populated minibands by using a sequential process, which consisted of the following steps: (1) determination of the characteristic width of the doped layer and of the doping period; (2) determination of the sheet carrier concentration n_S (this process outputs simultaneously the width, Δ_n, Fermi energy, ϕ_n, and dispersion factor, ϵ_n, for all minibands taken into consideration); (3) isolation of the magnetoresistance oscillations associated with individual minibands; and (4) determination of the quantum mobility of a populated miniband by fitting the appropriate equation [either Eq. (5) or (7)] to the isolated magneto-oscillatory component, with the quantum mobility being the single fitting parameter. In what follows, each of these steps is described in more detail.

A. Determination of the characteristic doping layer width and doping period

It has been shown by Ulrich *et al.*[22] that the C-V spectrum of a δ-doped semiconductor is very sensitive to the spreading of the impurity atoms. In order to estimate the characteristic width of the doped layer in our samples, we proceeded in the following way. Sample No. 187 with a single Si δ layer was grown under the same growth conditions used for the periodically δ-doped samples. In order to take advantage of the fact that the C-V technique presents a higher resolution for a higher sheet concentration of confined carriers, sample No. 187 was more highly doped than the other samples used in this work. The areal density of confined carriers in this sample was obtained from the Shubnikov–de Haas spectrum by following the prescription described in Ref. 5. Using the density of carriers obtained from the SdH spectrum, theoretical C-V profiles were generated by resolving self-consistently Schrödinger and Poisson equations for the structure under bias; in the calculation of the C-V spectrum, the doped layer was assumed to be of Gaussian profile, and the width of the Gaussian was varied until the theoretical C-V spectrum achieved best agreement with the experimental one. A more detailed description of the C-V technique and theory is presented in Ref. 2. Figure 1 shows the C-V spectrum for sample No. 187. The theoretical curve shown in Fig. 1 was calculated assuming the donor layer to be of width 8 Å, and it reproduces very well the experimental C-V spectrum. This demonstrates that Si atoms in the δ-doping layers in our samples are spread over not more than 2 ML of InP.

To determine the doping periods of a sample, its C-V spectrum was measured. As an example, the C-V spectrum for sample No. 200 is shown in Fig. 2. The C-V concentration, $N_{C\text{-}V}$, presents oscillations as a function of the C-V

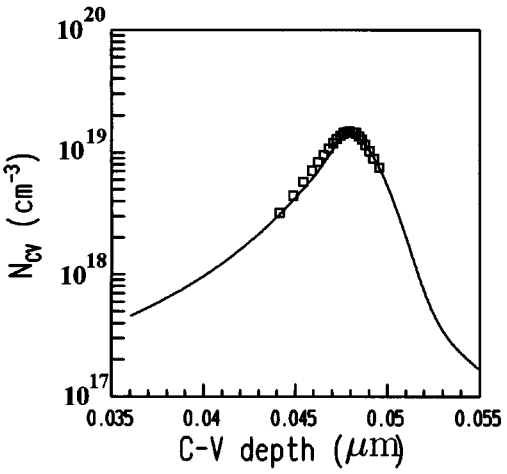

FIG. 1. Measured capacitance-voltage profile for sample No. 187 (square dots) for $T=300$ K. The theoretical C-V spectrum (full curve) was generated assuming $n_S=8.3\times10^{12}$ cm^{-2}, and the Si atoms distributed according to a Gaussian function of full width at half maximum of 8 Å.

depth, $z_{C\text{-}V}$. The oscillations seen in Fig. 2 display a periodicity of 176 Å, which we take to be equal to the doping period of this structure; the doping periods obtained in the same way are shown in Table I for all samples studied.

B. Determination of the carrier population and miniband parameters

The overall sheet carrier concentration n_S for each sample was extracted from an analysis of its Shubnikov–de Haas spectrum. Figure 3(a) shows the magnetoresistance spectrum for sample No. 196, and Fig. 3(b) shows the Fourier transform of the SdH oscillations plotted against the inverse field. Prior to taking the Fourier transform, and with the motive of reducing the unwanted background of monotonous magnetoresistance, the magnetoresistance curves were differentiated. Each of the peaks seen in Fig. 3(b) corresponds to a belly orbit of one of the populated minibands; the peak positions determine the belly extremal cross sectional areas of the mini-Fermi surface in units of $\hbar/2\pi e$.

To determine n_S it was necessary to solve self-consistently Schrödinger and Poisson equations [Eqs. (2) and (3)] for each sample. In the calculation, the doping period was fixed at the value determined by the C-V measurement, and the Si atoms were taken to be distributed according to a Gaussian function with a full width at half maximum of 8 Å as deduced from the C-V spectrum. The only additional parameter in this calculation, the carrier concentration n_S, was varied until all theoretical frequencies of magnetoresistance oscillation, i.e. those corresponding to the belly cross-sections of the mini-Fermi surface, approximated simultaneously all of the frequencies of oscillation seen in the experimental Shubnikov–de Haas spectrum. (It should be pointed out that such a procedure will incorporate into the final result of n_S those carriers in the outer minibands with a low-density population, which are beyond the sensitivity of the Shubnikov–de Haas spectrum). The procedure used to determine n_S is described in more detail in Ref. 23. Results of the analysis of the C-V spectra and of the Shubnikov–de Haas oscillations are summarized in Table I.

For samples with a period less than $\approx$200 Å quantum oscillations associated with miniband $E3$ were not observed. This is an indication that in this range of doping periods the minigap between minibands $E2$ and $E3$ is less than the broadening of the energy levels, meaning that for all practical purposes minibands $E3$ and $E2$ merge into a single energy band. Under these circumstances only the belly orbit associated with miniband $E2$ will be manifested by magnetoresistance oscillations which will follow the three-dimensional behavior described by Eq. (8). At still shorter periods ($d<150$ Å), miniband $E3$ becomes depleted of carriers.

In addition to the concentration of free carriers, the self-consistent calculations also output the Fermi energy ϕ_n, the width Δ_n, and the dispersion factor ϵ_n for all minibands; the parameters obtained are displayed in Table II.

C. Isolation of contributions of individual minibands to the magnetoresistance

Individual oscillatory components were separated from the rest of the magnetoresistance spectrum by applying a Fourier Gaussian bandpass filter; the bandpass filter param-

TABLE I. Parameters of the samples studied. The doping period d was obtained from the C-V spectrum of the sample. B_{Ei}^{SdH} and B_{Ei}^{Th} symbolize the experimental and theoretical frequencies of oscillation associated with the belly orbit in k space. The overall carrier concentration n_S shown gives the best agreement of theory with experiment.

Sample No.	No. of periods	d (Å)	SdH Experiment (T) B_{E1}^{SdH}	B_{E2}^{Sdh}	B_{E3}^{SdH}	Calculated (T) B_{E1}^{Th}	B_{E2}^{Th}	B_{E3}^{Th}	n_S (cm^{-2})
194	5	92.0	85.5	43.1		86.3	42.3		4.27×10^{12}
206	10	107	89.7	47.9		90.3	48.7		5.08×10^{12}
198	5	128	74.9	38.6		75.4	40.2		4.50×10^{12}
207	10	133	80.7	46.0		79.2	46.2		5.08×10^{12}
200	10	176	62.2	32.2		63.8	32.4	9.1	4.27×10^{12}
197	5	225	73.7	33.8		73.7	34.9	17.0	5.38×10^{12}
199	10	245	73.1	25.9	11.1	75.6	27.2	11.2	5.26×10^{12}
196	5	278	65.4	28.1	15.0	68.2	28.4	15.9	4.98×10^{12}
164	single		69.6	24.0	6.8	70.8	24.5	6.7	5.07×10^{12}

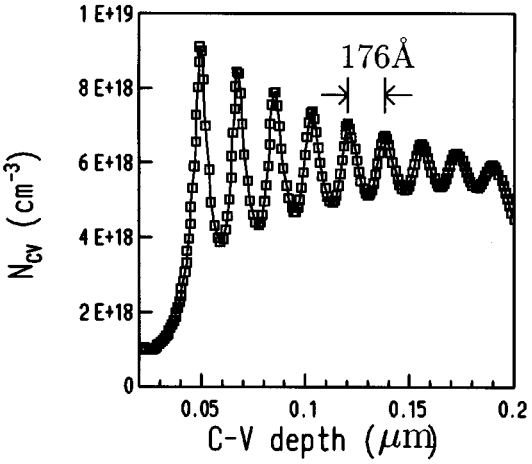

FIG. 2. Capacitance-voltage profile for sample No. 200. The periodicity of the peaks indicate that the doping period of this structure is 176 Å.

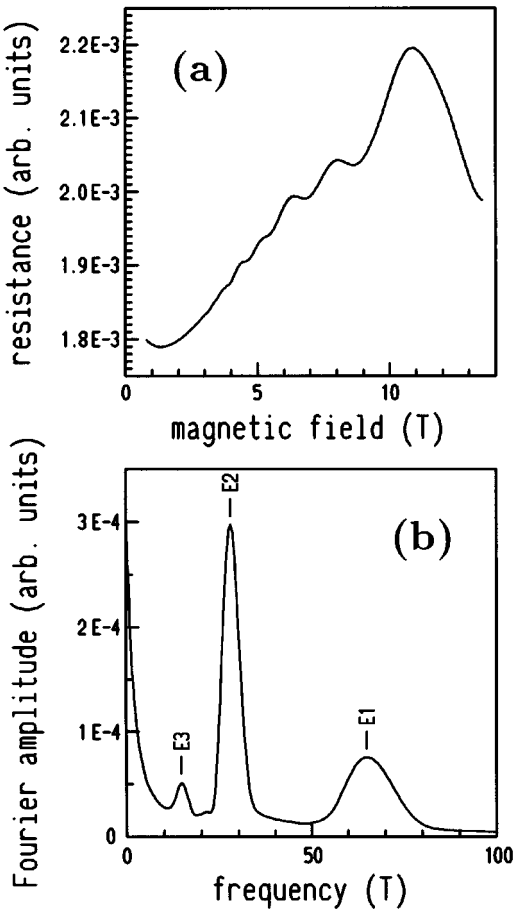

FIG. 3. (a) Shubnikov–de Haas spectrum of sample No. 196. (b) Fourier transform of the Shubnikov–de Haas spectrum plotted against $1/B$ and differentiated for sample No. 196. The frequencies of oscillation associated with the belly orbits are indicated.

eters were the peak frequency and full width at half maximum (FWHM). This is illustrated in Figs. 4(a)–4(d) for sample No. 196. We have chosen sample No. 196 to exemplify the results of the Fourier filtering procedure because in this sample each miniband is associated with one of the patterns which can be exhibited by the magneto-oscillatory components in periodically δ-doped semiconductors: the fundamental miniband $E1$ bears zero bandwidth and is thus two dimensional, giving a magnetoresistance contribution which will obey Eq. (7); miniband $E2$ bears a narrow bandwidth $\Delta_2 < \phi_2$, which corresponds to a dimensionality intermediate between 2 and 3, and its magnetoresistance oscillations will obey Eq. (5); and miniband $E3$, which has a large bandwidth $\Delta_3 > \phi_3$ is effectively three-dimensional, implying that its magnetoresistance oscillations will be described by Eq. (8). Thus sample No. 196 can serve the purpose of illustrating the Fourier filtering procedure and of the process of fitting individual oscillations with theory under all of the circumstances which can occur.

Figure 4(a) shows the Fourier transform of the SdH curve; dashed lines show the filtered Fourier transform, with bandpass filter parameters adjusted to isolate one of the Fourier peaks seen. After the application of the bandpass filter, all steps leading to the isolated Fourier transform were reversed: an inverse Fourier transformation was applied, and the magnetoresistance oscillations were integrated numerically. Figures 4(b)–4(d) shows the isolated magnetoresistance oscilla-

TABLE II. Miniband parameters obtained from the theoretical model. The energy width and the Fermi energy for each miniband, Δ_n and ϕ_n, respectively, are the values obtained from a self-consistent solution of Schrödinger and Poisson equations using d and n_S given in Table I. Parameter ϵ_n was obtained by fitting the numerically calculated dispersion law, $E_n(k)$, with Eq. (6), and it is indicated for minibands obeying the quasi-two-dimensional behavior of Eq. (5).

Sample No.	Δ_1 (meV)	ϕ_1 (meV)	ϵ_1	Δ_2 (meV)	ϕ_2 (meV)	ϵ_2	Δ_3 (meV)	ϕ_3 (meV)	ϵ_3
194	43.7	127.0	0.21	152.9	57.5			0.0	
206	26.4	130.2	0.16	105.8	68.8			0.0	
198	14.8	107.8	0.12	69.4	56.9			0.0	
207	11.0	118.3	0.09	61.0	64.0			0.0	
200	3.2	91.4	0.03	31.7	44.7			0.0	
197	2.8	107.1	0.00	11.4	45.4			0.0	
199	1.4	102.3	0.00	8.1	41.2	0.16		22.4	
196	0.0	95.5	0.00	4.6	35.9	0.11	19.9	19.0	
164	0.0	96.7	0.00	0.0	37.2	0.00	0.0	11.4	0.0

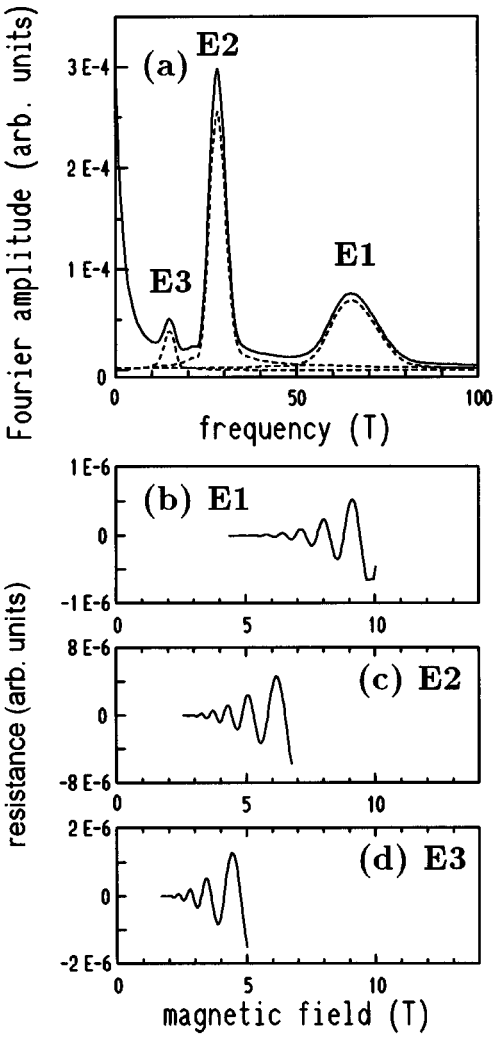

FIG. 4. (a) Fourier transform of the SdH spectrum for sample No. 196; dashed lines show the filtered Fourier transform used to isolate each of the peaks detected; (b)–(d) show the isolated oscillations due to minibands $E1$, $E2$, and $E3$, respectively.

tory components so obtained for sample No. 196. The isolated oscillations cover a smaller range of fields than the measured interval (0–14 T) because a certain interval at each end (the length of which is inversely proportional to the FWHM of the Fourier filter) is lost due to end effects (see, for instance, Ref. 24).

D. Experimental estimates for the quantum mobilities

The quantum mobility associated with each of the populated minibands was obtained from a fit with theory of the minibands' contribution to the magnetoresistance, isolated from the rest of the Shubnikov–de Haas spectrum as described in Sec. IV C. The individual oscillations were fitted using Eq. (5) when the miniband energy width was narrow ($\Delta_n < \phi_n$), or Eq. (8), when the miniband width was wide ($\Delta_n > \phi_n$). Parameters Δ_n, ϕ_n, and ϵ_n used in the fitting equation were fixed at the values given in Table II and the temperature was set to 4.2 K, as used in our experiments. The only remaining parameter, $\mu_Q(n)$, was adjusted for best agreement with the experiment. To illustrate the fitting procedure, the individual oscillations and the fitted

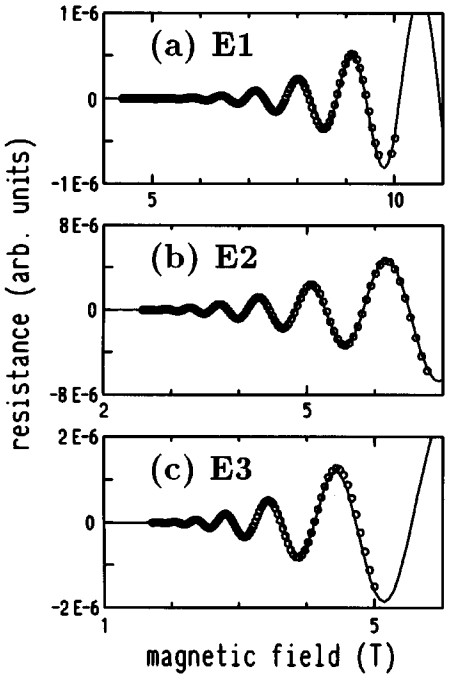

FIG. 5. Magnetoresistance oscillations associated with individual minibands for sample No. 196. Dots represent the oscillations obtained experimentally and the full curves correspond to the theory. (a) Isolated oscillations due to the fundamental miniband, $E1$ and theoretical result by use of Eq. (5). (b) Same for miniband $E2$. (c) Isolated oscillations due to miniband $E3$ and theoretical result obtained by use of Eq. (8).

curves for sample No. 196 are shown in Fig. 5; a fit with theory in this case yielded $\mu_Q(E1)=410$ cm^2/V s, $\mu_Q(E2)=1320$ cm^2/V s, and $\mu_Q(E3)=3650$ cm^2/V s. All other samples underwent the same treatment, and the quantum mobility values obtained are plotted against doping period in Fig. 6.

V. COMPARISON WITH THEORY AND DISCUSSION

Experimental results showed that at a fixed doping period the quantum mobility increases with the index of the mini-

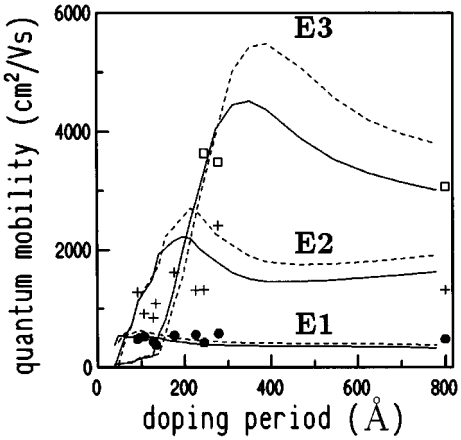

FIG. 6. Quantum mobility as a function of the doping period. Circles, crosses, and squares represent the experimental results corresponding to minibands $E1$, $E2$, and $E3$, respectively; dashed and full lines depict the theoretical result for $n_S=4.3\times10^{12}$ and 5.4×10^{12} cm^{-2}, respectively.

band. The experimental quantum mobilities associated with individual minibands are shown by dots in Fig. 6 as a function of the doping period d. At large values of d adjacent wells become uncoupled; the quantum miniband mobilities obtained for sample No. 164, which contains a single δ layer, is plotted in Fig. 6 at $d=800$ Å.

When the period is made shorter, the mobility in miniband $E1$ remains nearly unchanged. The experimental quantum mobility in miniband $E2$ does not show a smooth dependence on the doping period, which is attributed to the fluctuation in carrier density in the samples (see Table I) and to the limited accuracy of the experimental values of mobility. Nevertheless, the experimental data plotted in Fig. 6 shows clearly that in the region $d<200$ Å the $E2$ quantum mobility decreases when the doping period is made shorter. Finally, the quantum mobility of carriers in miniband $E3$ could only be measured for periods greater than 230 Å, in which range the measured mobility attains a value of approximately 3500 $\mathrm{cm}^2/\mathrm{V\,s}$.

The theoretical quantum mobilities were calculated as a function of the doping period for carrier concentrations of $n_S=4.3\times10^{12}$ and 5.4×10^{12} cm^{-2}; these values correspond to the lower and upper limits of the free-carrier concentration in the samples studied. The input quantities were the Fermi energy, miniband energy spectrum, and wave functions, which were obtained from the solution of Schrödinger and Poisson equations as described in Sec. IV B. The quantum mobilities were calculated by using Eq. (4), assuming periodic boundary conditions in an interval of four doping periods, and incorporating into the calculations only the quantum states belonging to the three lowest energy minibands. Results of the theory are shown by lines in Fig. 6.

Figure 6 shows that for miniband $E1$ the theoretical quantum mobilities are in excellent agreement with the experimental ones. For excited minibands $E2$ and $E3$ there is an order-of-magnitude agreement between theory and experiment, although the overall agreement is not so good as for miniband $E1$. Nevertheless, it is to be noticed that the theory reproduces the main feature of the $E2$ quantum mobility dependence on d, i.e., a decrease toward short superlattice periods.

Our investigation can be summarized by stating that, at a given superlattice period, the quantum mobility is higher in more energetic minibands, and when the period is made shorter, the quantum mobilities decrease. The decreasing behavior toward short superlattice periods develops at $d\sim300$ Å for miniband $E3$, but only at $d\sim200$ Å for miniband $E2$; for miniband $E1$, theory predicts a decreasing behavior only when $d<50$ Å. These results can be explained by the dependence of the binding length of carriers on the doping period d. As shown in Ref. 12 for δ-doped samples with a single doping layer and in Ref. 13 for gated δ-doped samples, the mobility is very sensitive to the mean distance between the impurity layer and the charge carriers. The mean distance between carriers confined in miniband Ei and an impurity layer at $z=0$ can be estimated by $\sqrt{\langle z^2\rangle_{Ei}}$, where

$$\langle z^2\rangle_{Ei}=N\int_{-d/2}^{+d/2} z^2|u_i(k_{\mathrm{Belly}},z)|^2dz\ . \tag{9}$$

A plot of $\sqrt{\langle z^2\rangle_{Ei}}$ for a carrier density of $n_S=4.6\times10^{12}$ $\mathrm{cm}^2/\mathrm{V\,s}$ is shown in Fig. 7. A comparison of Figs. 7 and 6 shows that there is an outstanding correlation between the quantum mobility in a miniband, and the mean distance between its carriers and an impurity sheet.

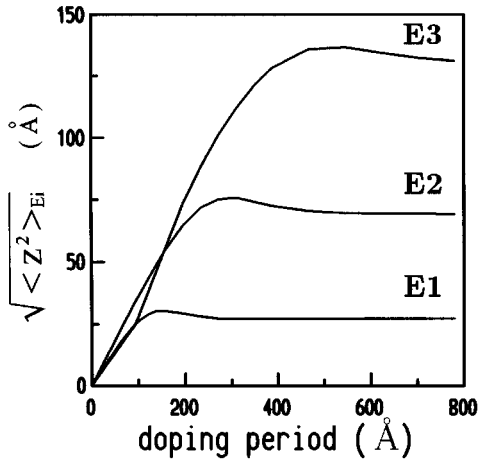

FIG. 7. Mean distance between carriers confined in minibands $E1$, $E2$, and $E3$ as a function of the doping period for periodically δ-doped InP with $n_S=4.6\times10^{12}$ $\mathrm{cm}^2/\mathrm{V\,s}$. The calculation was made using Eq. (9).

VI. CONCLUSION

The Shubnikov–de Haas oscillations were measured for periodically δ-doped InP as a function of the doping period in samples with a density of carriers around $\sim4.9\times10^{12}$ cm^2 per doped layer and doping period in the range 90–300 Å. It is verified that each miniband manifests itself in the SdH spectrum through a single oscillatory component, which corresponds to the belly extremal orbit of its mini-Fermi surface. The quantum oscillations associated with individual minibands were isolated from the underlying magnetoresistance spectrum by Fourier techniques. From the individual oscillatory components, the quantum mobility for each miniband was estimated.

A theoretical model for the quantum mobility was developed, which yields a fair agreement with the experimental results. The theoretical model predicts that the mobilities will increase with the miniband index, and the mobilities decrease when the doping period is made shorter. The onset of the decreasing behavior occurs at $d\sim200$ Å for miniband $E2$, and below $d\sim50$ Å for miniband $E1$. The dependence of the quantum mobility in an individual miniband on the distance between dopant sheets shows a salient correlation with the same dependence of the mean distance between its carriers and the doped layer. This demonstrates that the mean distance between confined carriers and impurities is the determinant of the absolute value of carrier mobility which can be achieved in δ-doped systems.

ACKNOWLEDGMENTS

Calculations were performed using the facilities of the Laboratório de Computação Científica Avançada da Universidade de São Paulo (LCCA-USP). A.B.H. acknowledges support by FAPESP, Grant No. 94/5645-7, and CNPq, Grant No. 306335/88.

[1] E. F. Schubert, *Doping in III-V Semiconductors* (Cambridge University Press, Cambridge, 1993), p. 433.
[2] E. F. Schubert, in *Epitaxial Microstructures*, edited by A. C. Gossard, Semiconductors and Semimetals Vol. 40 (Academic Press, New York, 1994), p. 1.
[3] R. Droopad, S. D. Parker, E. Skuras, R. A. Stradling, R. L. Williams, R. B. Beall, and J. J. Harris, in *High Magnetic Fields in Semiconductor Physics II*, edited by G. Landwher (Springer-Verlag, Berlin, 1989), p. 199.
[4] S. Yamada and T. Makimoto, Appl. Phys. Lett. **57**, 1022 (1990).
[5] P. M. Koenraad, B. F. A. van Hest, F. A. Blom, R. van Dalen, M. Leys, J. A. A. J. Perenboom and J. H. Wolter, Physica B **177**, 485 (1992).
[6] O. Mezrin and A. Shik, Superlatt. Microstruct. **10**, 107 (1991).
[7] O. A. Mezrin, A. V. Shik, and V. O. Mezrin, Semicond. Sci. Technol. **7**, 664 (1992).
[8] L. R. González, J. Krupski, and T. Szwacka, Phys. Rev. B **49**, 11 111 (1994).
[9] G. -Q. Hai, N. Studart, and F. M. Peeters, Phys. Rev. B **52**, 8363 (1994).
[10] G. -Q. Hai and N. Studart, Phys. Rev. B **52**, R2245 (1995).
[11] P.M. Koenraad, A. F. W. van de Stadt, J. M. Shi, G. Q. Hai, N. Studart, P. Vansant, F. M. Peeters, J. T. Devreese, J. A. A. J. Perenboom, and J. H. Wolter, Physica B **211**, 426 (1995).
[12] A. B. Henriques, Phys. Rev. B **53**, 16 365 (1996).
[13] L. C. D. Gonçalves and A. B. Henriques, Semicond. Sci. Technol. **12**, 203 (1997).
[14] D. Schneider, D. Rürup, A. Plichta, H. Grubert, A. Schalchetzki, and K. Hansen, Z. Phys. B **95**, 281 (1994).
[15] D. K. Schroder, *Semiconductor Material and Device Characterization* (Wiley, New York, 1990), p. 43.
[16] L. Hedin and B. Lundqvist, J. Phys. C **4**, 2064 (1971).
[17] R. Fletcher, E. Zaremba, M. D'Iorio, C. T. Foxon, and J. J. Harris, Phys. Rev. B **41**, 10 649 (1990).
[18] A. B. Henriques and L. C. D. Gonçalves, Semicond. Sci. Technol. **8**, 585 (1993).
[19] A. B. Henriques, Phys. Rev. B **50**, 8658 (1994).
[20] P. T. Coleridge, R. Stoner, and R. Fletcher, Phys. Rev. B **39**, 1120 (1989).
[21] L. M. Roth and P. N. Argyres, in *Physics of III-V Compounds*, edited by R. Willardson and A. Beer, Semiconductors and Semimetals Vol. 1, (Academic Press, New York, 1996), p. 159.
[22] B. Ulrich, E. F. Schubert, J. B. Stark, and J. E. Cunningham, Appl. Phys. A **47**, 123 (1988).
[23] A. B. Henriques, L. C. D. Gonçalves, P. L. Souza, and B. Yavich, Semicond. Sci. Technol. **11**, 190 (1996).
[24] W. H. Press, B. P. Flannery, A. A. Teukolsky, and W. T. Vetterling, *Numerical Recipes* (Cambridge University Press, New York, 1987), pp. 407–411.